

FROM THE CURRENT LITERATURE

PACS number: **74.72. – h**

Tunneling effects in highly anisotropic layered superconductors

T B Charikova, N G Shelushinina, V N Neverov, M R Popov

DOI: https://doi.org/10.3367/UFNe.2023.11.039604

Contents

Abstract. A brief review of the galvanomagnetic properties of highly anisotropic cuprate superconductors is presented, with an emphasis on the internal Josephson effect, which naturally exists in multilayer HTSC crystals. The transport of charge carriers perpendicular to the layers in such materials occurs by successive tunneling of quasiparticles (or Cooper pairs) between highly conducting (or superconducting) CuO_2 layers through intermediate buffer layers. Currently available results on the nonmetallic conductivity along the *c*-axis in the normal state are analyzed, as are data on the distinctive branched current-voltage characteristics in the superconducting state, which are clear experimental manifestations of tunneling effects in layered cuprate superconductors.

Keywords: layered superconductors, tunneling effects, current-voltage characteristic, internal Josephson effect

1. Introduction

Oxide superconductors are layered compounds with building blocks, consisting of conducting layers of CuO_2 and separated by buffer layers that serve as charge reservoirs (see monographs [1–4] for a detailed description).

Strongly anisotropic high-temperature superconductors (HTSCs) can be considered a 'pack' of CuO_2 superconducting layers, coupled by Josephson interactions [5–8]. New properties of these materials compared to single Josephson junctions are due to their multilayer structure and the atomic thickness of superconducting layers.

In the case of weak anisotropy, a description in terms of continuous anisotropic Ginsburg–Landau or London theory is applicable. On the other hand, at strong anisotropy, the discreteness of the structure becomes relevant, and a description in terms of a set of weakly coupled superconducting layers, which is provided by a discrete model proposed by Lawrence and Doniach, is applicable [5].

The general Lawrence–Doniach model is a basis for discussing the physics of multilayer systems: from weakly anisotropic three-dimensional ones to strongly anisotropic layered and even two-dimensional superconductors (see, e.g., [1, 6–8]). The criterion of transition from a continuously anisotropic to discrete-layered description is the smallness of the coherence length ξ_c along the *c*-axis with respect to the separation *d* between the layers.

Generally, the continuous anisotropic description is applicable to $YBa_2Cu_3O_{7-x}$ (YBCO) [9] in a wide temperature range, whereas the layered compounds of Bi and Tl belong to the class of materials with $\xi_c(T=0) < d$ and, therefore, the Lawrence–Doniach model is applicable to them. The most anisotropic high-temperature superconductors are multilayered systems, in which the superconducting CuO_2 layers are separated by barrier layers. Examples are $Bi_2Sr_2CaCu_2O_8$ (BSCCO) or $Tl_2Ba_2Ca_2Cu_3O_{10}$ (TBCCO) systems.

The commonly accepted criterion of a transition from a continuous anisotropic to discrete layered description is the smallness of the coherence length along the *c*-axis, ξ_c, relative to the interlayer separation *d*, expressed by the dimensionless ratio $\tau_c = 2\xi_c^2(0)/d^2$ [8].

The ratio τ_c characterizes the transition from quasi-two-dimensional layered to continuous three-dimensional anisotropic behavior:

- for large coherence length $\xi_c(0)$, i.e., for $\tau_c \gg 1$, the continuous description is always relevant;
- on the other hand, for small $\tau_c \ll 1$ at a temperature of $T_{cr} = (1-\tau_c)T_c < T_c$, a crossover will take place, at which

T B Charikova [(a)], **N G Shelushinina** [(b)], **V N Neverov** [(c)], **M R Popov** [(d)]
Mikheev Institute of Metal Physics,
Ural Branch of the Russian Academy of Sciences,
ul. S Kovalevskoi 18, 620108 Ekaterinburg, Russian Federation
E-mail: [(a)] charikova@imp.uran.ru, [(b)] shel@imp.uran.ru,
[(c)] neverov@imp.uran.ru, [(d)] popov_mr@imp.uran.ru

Received 18 September 2023, revised 7 November 2023
Uspekhi Fizicheskikh Nauk **194** (7) 740 – 752 (2024)
Translated by V L Derbov

the system behaves in a quasi-two-dimensional way at low temperatures, $T < T_{cr}$, and demonstrates three-dimensional anisotropic behavior at $T > T_{cr}$.

The transport between the layers occurs through sequential tunneling of charge carriers and, therefore, the appropriate multilayer structures can be considered a set of intrinsic Josephson tunnel junctions. The main focus in this article will be on tunneling effects both in normal (tunneling of quasiparticles) and in superconducting (tunneling of Cooper pairs) states of a HTSC system.

2. Tunneling of quasiparticles in normal phase of a layered superconductor

2.1 Nonmetallic behavior of conductivity along *c*-axis: dependences $\rho_c(T)$ (experiment)

The issues of charge transport in various crystallographic directions (in the *ab* plane and in the direction of the crystal *c*-axis) in cuprates as well as the problem of superconduction in multilayer anisotropic systems are undoubtedly of great interest. Early work in this area was already devoted to the study of the anisotropy of the transport properties of layered cuprate systems in the normal state. The studies were carried out with various materials: YBCO [9–12], $La_{2-x}Sr_xCuO_4$ (LSCO) [13–15], and $Bi_2Sr_{2-x}Ca_xCu_2O_8$ (BSCCO) [16].

The specific resistance in various directions differs not only by magnitude but also by the character of temperature dependence. Metallic behavior in the conducting planes and nonmetallic behavior in the *c* direction have been attracting the attention of theorists for a long time [17–19].

The combination of a nonmetallic type of temperature dependence of resistance along the *c*-axis, $d\rho_c(T)/dT < 0$, with the metallic conductivity in the *ab*-plane, $d\rho_{ab}(T)/dT > 0$, in the presence of strong anisotropy of conducting properties, $\rho_c/\rho_{ab} \gg 1$, has been multiply observed in underdoped and optimally doped HTSCs [20]. This is a manifestation of the quasi-two-dimensionality of oxide systems consisting of high-mobility CuO_2 layers separated by buffer layers. Examples of nonmetallic temperature dependence of the resistance ρ_c are shown in Fig. 1 for hole-doped cuprates YBCO [21] and BSCCO [22], for the magnetic superconductor $RuSr_2GdCu_2O_8$ (RSGCO) [22], and for the iron-based HTSC $(V_2Sr_4O_6)Fe_2As_2$ ((VSrO)FeAs) [23], as well as in Fig. 2 for the electron-

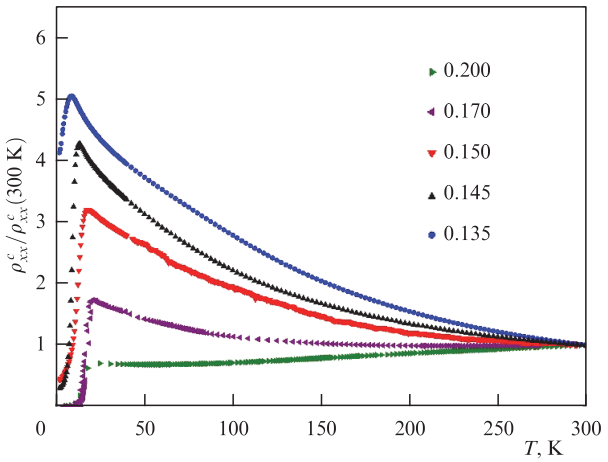

Figure 2. Temperature dependences of specific resistance along *c*-axis for $Nd_{2-x}Ce_xCuO_4/SrTiO_3$ $(1\bar{1}0)$ films with various contents of Ce in relative units [22].

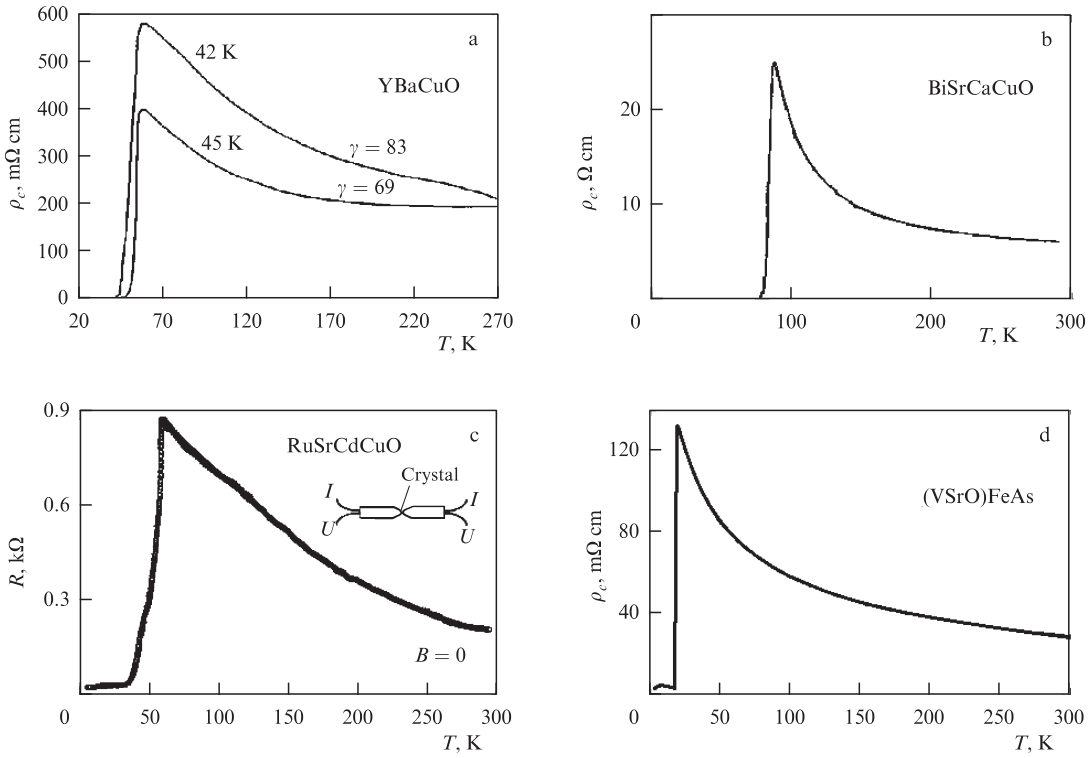

Figure 1. Temperature dependence of resistance along *c*-axis: (a) for two oxygen-depleted $YBa_2Cu_3O_{7-\delta}$ mesa structures. Critical temperatures T_c and anisotropy coefficients γ [21] are indicated; (b) for $Bi_2Sr_2CaCu_2O_{8+\delta}$ single crystal annealed in argon, $T_c = 86$ K [24]; (c) for $RuSr_2GdCu_2O_8$ single crystal. Inset presents a schematic diagram of contacts with the samples [25]; (d) for slightly underdoped samples of $(V_2Sr_4O_6)Fe_2As_2$, $T_c = 19$ K. Growth of resistance when decreasing temperature indicates isolating character of VSr_2O_3 blocks between superconducting layers of FeAs [23].

doped cuprate $Nd_{2-x}Ce_xCuO_4$ (NCCO) with various content of the doping impurity (x) studied by us [22].

2.2 Model of incoherent tunneling of charge carriers

The nonmetallic behavior of $\rho_c(T)$ and the large anisotropy of resistance are associated with incoherent tunneling of charge carriers in the c direction [26, 27]. The incoherent transfer between CuO_2 planes occurs when the probability of carrier scattering in the plane, $1/\tau$, is much greater than the transfer integral $t_c(\equiv 1/\tau_{esc})$ between the planes: $\tau_{esc}/\tau \gg 1$. Here, τ is the relaxation time of charge carriers in the plane and τ_{esc} is the time of escape from the given plane to a neighboring one. If an electron undergoes many collisions before moving to another plane, then the sequential processes of interplane tunneling are not correlated.

From the expressions for the diffusion coefficient along ($D_{||}$) and across ($D_\perp$) the planes, $D_{||} = l^2/2\tau$ and $D_\perp = d^2/\tau_{esc}$, where l is the free path length in the ab-plane and $d = 6$ Å is the separation between the neighboring CuO_2 layers, it is possible to evaluate the ratio of characteristic times:

$$\frac{\tau_{esc}}{\tau} \cong \left(\frac{d}{l}\right)^2 \frac{D_{||}}{D_\perp} \sim \left(\frac{d}{l}\right)^2 \frac{\rho_c}{\rho_{ab}}\,. \tag{1}$$

For a quantitative description of the dependence $\rho_c(T)$, the model of a natural superlattice is used, in which the CuO_2 layers are quantum wells and the buffer layers are barriers with height Δ [28–31]. Figure 3 schematically presents structures of BSCCO (with two CuO_2 layers in a unit cell) and NCCO (with one CuO_2 layer per unit cell) crystals.

In this model, the tunneling matrix element has the form

$$t_c = \exp\left(-d\sqrt{\frac{2m\Delta}{\hbar^2}}\right). \tag{2}$$

The higher the temperature, the more essential the role of the contribution to conductivity related to the thermal activation of carriers through the barrier. Therefore, to describe the nonmetallic behavior of $\rho_c(T)$ quantitatively, it is necessary to consider both the interlayer tunneling along the c-axis and the thermal activation of carriers over the barriers. Giura et al. [29, 30] presented a phenomenological model for electric charge transport along the c-axis based on the existence of two energy barriers in double-layer cuprates $Bi_2Sr_2CaCu_2O_{8+\delta}$ (BSCCO) (Fig. 3a).

In Refs [29, 30], it is assumed that two complementary processes determine the conductivity along the c-axis, namely, the incoherent tunneling, $\sigma_c^{tun} \sim t_c^2$, and the thermal activation through the barriers, $\sigma_c^{th}(T) \sim \exp(-\Delta/kT)$. In Ref. [22], we applied this model to describe the temperature dependence of the conductivity $\sigma_c(= 1/\rho_c)$ in single-crystal NCCO films with one layer of CuO_2 per unit cell, i.e., for the case of barriers of one type only (Fig. 3b).

Within the framework of the proposed model, by fitting the parameters Δ, it turns out to be possible to describe the dependence $\sigma_c(T)$ both for BSCCO crystals [29, 30] and for NCCO films with various contents of cerium [22] at $T \geqslant (50-100)$ K. However, at lower temperatures, this model is not sufficient.

In Ref. [22], experimental results are presented on the nonmetallic temperature dependence of the resistance along the c-axis, $\rho_c(T)$, for epitaxial films of electron-doped $Nd_{2-x}Ce_xCuO_4$ superconductor grown on $(1\bar{1}0)$ $SrTiO_3$ single-crystal substrate within a wide range of cerium content in an optimal annealing regime.

An analysis of the temperature dependence $\rho_c(T)$ for a set of $Nd_{2-x}Ce_xCuO_4/SrTiO_3$ samples with $x = 0.12 - 0.17$ leads to the empirical expression

$$\rho_c(T) = \rho_0 + \rho_1 \exp\left(-\frac{kT}{\Gamma}\right), \tag{3}$$

where ρ_0, ρ_1, and the characteristic energy scale Γ are fitting parameters.

Figure 4 shows the dependences $\rho_c(T)$ for NCCO single-crystal films with $x = 0.145$ and 0.15 from Ref. [22], as well as the corresponding fit of these dependences using Eqn (3). It can be seen that Eqn (3) describes with remarkable accuracy the experimental data within the range from $T = T_c$ to $T = 300$ K. The obtained values of parameters ρ_0, ρ_1, and Γ are presented in the figures.

One of the consequences of Eqn (3) is that, at $T \to 0$ (in the absence of superconductivity), the resistance along the c-axis would tend to a finite value $\rho_c(T \to 0) \to \rho_0 + \rho_1 = \text{const}$ (Fig. 4). Physically, this can mean the decisive role of subbarrier tunneling in the charge transport along the c-axis, especially at low temperatures.

Figure 5 presents examples of applying empirical relation (3) obtained by us to describe the experimental dependences $\rho_c(T)$ for other HTSC compounds: two samples of YBaCuO, BiSrCaCuO single crystal, as well as (VSrO)FeAs pnictide (the initial data for these samples are presented above in Fig. 1). In some cases, the dependence of the form

$$\rho_c(T) = a + \frac{b}{T}\,, \tag{4}$$

with the coefficients a and b as fitting parameters, is presented for comparison.

In 1988, Anderson and Zou [17] derived the dependence $\Delta\rho_c(T) \sim 1/T$ for a nontraditional transport mechanism in cuprates, determined by the charge carrier localization in CuO_2 planes (layers) with strong restriction (confinement) of

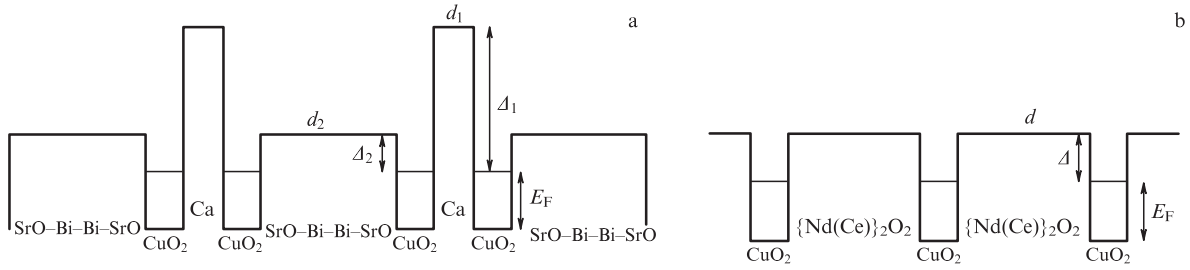

Figure 3. Schematic of well and barrier geometries in natural superlattice model (a) for BSCCO crystal [29] and (b) for NCCO crystal [22].

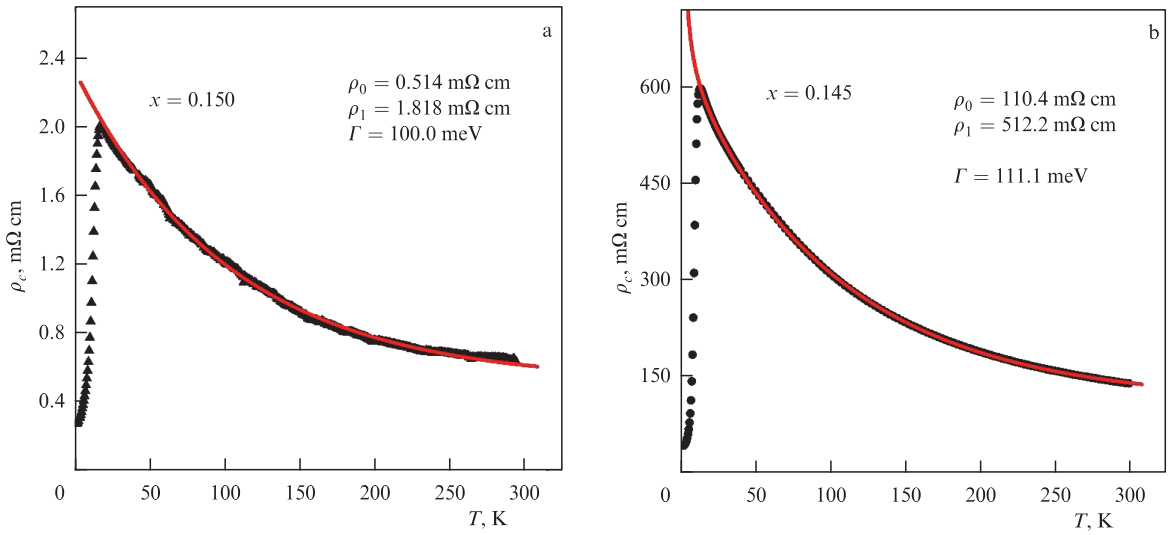

Figure 4. Temperature dependences of specific resistance along c-axis for (a) optimally ($x = 0.150$) and (b) almost optimally ($x = 0.145$) doped $Nd_{2-x}Ce_xCuO_4/SrTiO_3$ ($1\bar{1}0$) films with an approximation of experimental dependences using expression (3) (red curves).

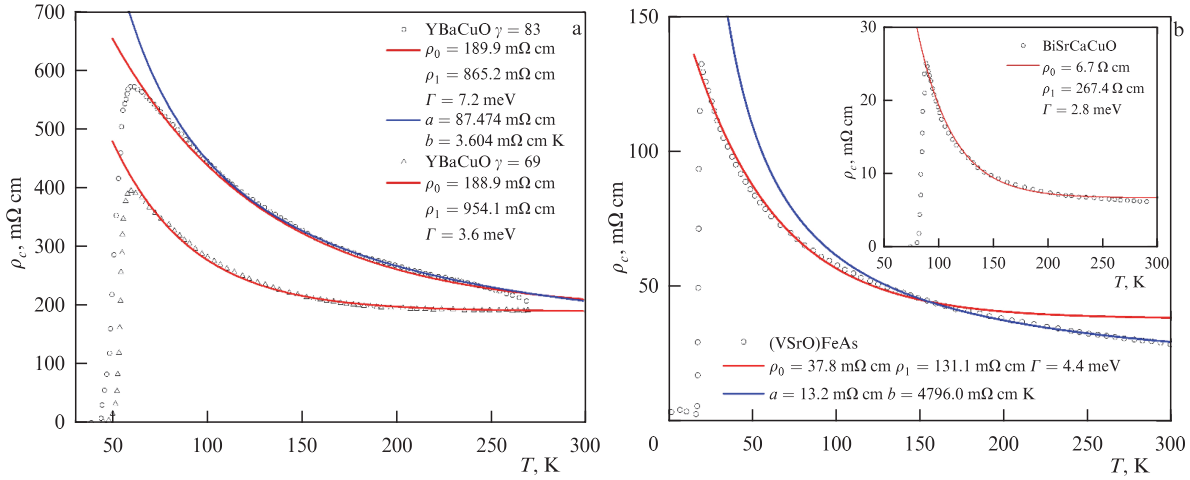

Figure 5. Approximation of experimental dependences $\rho_c(T)$ using expressions (3) (red curves) and (4) (blue curves) for YBaCuO (a), (VSrO)FeAs (b), and BiSrCaCuO (inset in Fig. b).

their motion in the c-direction. A dependence of such a form allows a qualitative description of experimental data on $\rho_c(T)$ for a wide range of HTSC compounds (see, e.g., Ito et al. [20]).

From Fig. 5, it is seen that Eqn (3) adequately describes experimental data for all presented samples in a wide range of temperatures from $T = T_c$ to $T = 300$ K (except $T > 150$ K for pnictide).

On the other hand, the Anderson law (4) generally provides a good description of experimental dependences, except the region of low temperatures $T < (100-150)$ K. In this temperature region, which is of critical importance for understanding the nature of charge transport along the c-axis in layered HTSCs, expression (3) has an undoubted advantage in accuracy in describing the presented data, although there is still no theoretical explanation for such a dependence.

3. Intrinsic Josephson effect (tunneling of Cooper pairs)

Most HTSC theoretical models assume the properties of layered cuprates with a high critical temperature in both the normal and superconducting state to be determined by the properties of CuO_2 layers, whereas other structure components in a unit cell act as reservoirs of charge. The importance of the interlayer coupling mechanism (in the c-axis direction) was particularly emphasized even at the early stage of cuprate HTSC studies, when a model of interlayer tunneling was developed by Anderson [32]. In this model, the tunneling processes along the c-axis are considered in both the superconducting (tunneling of Cooper pairs) and normal state (single-particle tunneling) of a layered superconductor.

Due to the layered structure and, therefore, strong anisotropy, a crystal of high temperature cuprate in the superconducting state can be considered a stack of tunnel Josephson junctions. These junctions are called intrinsic Josephson junctions (IJJs) [33, 34]. The intrinsic Josephson effect as the tunneling of Cooper pairs between neighboring CuO_2 planes in a strongly anisotropic layered HTSC is an integral part of many theories on the issue (see, e.g., reviews [33, 34] and numerous references therein).

The fact that intrinsic tunneling of Cooper pairs really takes place has been experimentally confirmed for many cuprate systems: for $Bi_2Sr_2CaCu_2O_8$ (BSCCO) [33–37], $Bi_2(Sr_{2-x}La_x)CuO_6$ (BSLCO) [38], $Tl_2Ba_2Ca_2Cu_3O_{10}$ (TBCCO) [24], $La_{2-x}Sr_xCuO_4$ (LSCO) [38], and electron-

doped cuprates $Pr_{2-x}Ce_xCuO_4$ (PCCO) [39] and $Sm_{2-x}Ce_xCuO_4$ (SCCO) [40], as well as the magnetic superconductor $RuSr_2GdCu_2O_8$ (RSGCO) [25].

In these experiments, both DC and AC Josephson effects were observed. If the supercurrents along the *c*-axis are limited by the Josephson effect, one should consider experimentally a series of tunneling processes (semiconductor–isolator–semiconductor (SIS)) or closeness effects (superconductor–normal metal–superconductor (SNS)) in Josephson junctions.

The studies of current-voltage ($I-V$) characteristics for the current along the *c*-axis, including the analysis of temperature dependence of the critical current $I_c(T)$, have clearly shown that all materials behave like a set of Josephson junctions: superconductor–dielectric–superconductor [21, 24, 25, 35, 38–41]. These experimental data are of primary importance, since they impose limitations on the possible theories of high-temperature superconductivity [33].

3.1 Resistive model of Josephson junctions

In 1962, Josephson [42] made a remarkable prediction that a nondamping (dissipation-free) superconduction current (supercurrent) can flow through a tunnel junction between two superconductors (a contact of superconductors through a thin isolating interlayer, SIS junction) in the absence of external applied voltage:

$$I_s = I_c \sin \Delta\varphi\,; \tag{5}$$

here, I_c is the critical current (the maximum value of supercurrent that can be supported by a Josephson junction), and $\Delta\varphi$ is the phase difference of the order parameter (the Ginsburg–Landau wave function) at two banks of the junction (with the resistance R):

$$I_c = \frac{\pi \Delta_0^2}{4eT_c R}\,, \tag{6}$$

where Δ_0 is the superconducting gap, and T_c is the critical temperature.

This is the first Josephson effect, the *DC* one. The term *Josephson effect* at present is used for a set of phenomena that take place in junctions of two superconductors through weak coupling (see, e.g., the review by Likharev [43], as well as books by Tinkham [3] or Schmidt [44]).

The typical cases of superconducting (S) structures with weak coupling are the tunneling SIS structure with the insulator (I) interlayer proposed by Josephson [42], the SNS structure with a thin interlayer of normal (N) metal (with weak superconductivity due to the closeness effect), or the ScS junction, where 'c' denotes the region of short constriction in a bulk superconducting material (e.g., a film), etc.

Josephson effect in a tunnel SIS junction. Consider the simplest (and historically the first) type of Josephson junction — two superconductors separated by a thin layer of dielectric. Such a junction is referred to as tunnel or SIS junction. For electrons, the dielectric layer is a potential barrier, and, if the layer is thin enough, there is a finite probability of their penetration through it by quantum tunneling. Even if the transmission coefficient of the barrier is small, its difference from zero is of fundamental importance, because phase matching of wave functions occurs (phase coherence is established) between two superconductors, both superconductors becoming a united system described by one condensate wavefunction.

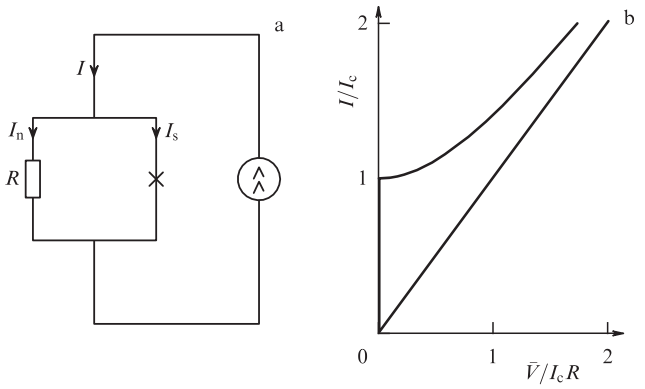

Figure 6. (a) Resistive model of a Josephson junction connected in a circuit with current supply. Josephson junction is indicated by an '×'. Total current I consists of superconducting current $I_s = I_c \sin\varphi$ and normal dissipative current I_n [45]. (b) Current-voltage characteristic of a Josephson junction. Voltage across junction occurs when $I > I_c$ [46].

This circumstance it what gives rise to the Josephson effect: the unity of the condensate wavefunction means that a superconduction current can flow through the junction between two superconductors even in the absence of external applied voltage.

From the time of its discovery [42], the Josephson effect has been one of the most remarkable manifestations of quantum coherence on a macroscopic scale, with a variety of technological applications [45].

Experimentally, a situation is often studied when the junction is in the mode of a given current, while the voltage on it is determined by the properties of the system. Until the given current I is less than the critical current I_c, all the current is superconducting, $I = I_s$. If $I > I_c$, then, in addition to the supercurrent, a normal current component I_n arises, subject to dissipation, and, therefore, some voltage V appears on the junction.

In this case, it is important that the voltage V arising on the junction periodically depends on time with frequency $\omega = (2e/\hbar)R\sqrt{I^2 - I_c^2}$, where R is the junction resistance in the normal state. Consequently, the Josephson junction begins to radiate electromagnetic waves; this phenomenon is called *Josephson generation* (the second, *AC,* Josephson effect).

The AC Josephson effect can be considered within the framework of the so-called resistive model (see, e.g., [44] and [46]): the Josephson junction is presented as a parallel connection of an ideal (nondissipative) Josephson junction and a resistor R (Fig. 6a). Then, the total current I through the system is a sum of the supercurrent I_s, determined by Eqn (5), and the normal current $I_n = V/R$. A DC voltmeter connected to the junction will show the mean (time-averaged) voltage $\bar{V}$, and the appropriate current-voltage characteristic will have the form

$$\bar{V} = R\sqrt{I^2 - I_c^2}\,, \tag{7}$$

shown in Fig. 6b.

If the current I only slightly exceeds I_c, then the current mainly flows as a supercurrent through the Josephson element in the equivalent circuit in Fig. 6a, whereas the normal current I_s is small. On the contrary, at $I \geqslant I_c$, almost all the current flows through the resistor ($I \approx I_n$), and the current-voltage characteristic at this segment goes to the linear characteristic of the junction in the normal state.

Experimental studies of the effects of tunneling charge carriers along the c-axis in strongly anisotropic HTSCs have clearly shown that all materials behave like a set of Josephson superconductor–isolator–superconductor junctions (see references above). The adjacent superconducting layers in a high-temperature superconductor are weakly coupled by the Josephson effect, because of which single crystals, in fact, act as vertical stacks of hundreds of Josephson junctions.

The current-voltage characteristics (CVCs) for the current flowing in the direction of the c-axis demonstrate a series of sequential Josephson junctions: they have many resistive branches and clearly expressed hysteresis. Typical CVCs for some layered HTSC systems will be demonstrated in Section 3.2. The current-voltage characteristics of the set of Josephson tunnel junctions consist of several branches, each of them corresponding to one, two, three, etc. individual junctions, transiting to the quasiparticle (normal) state, as the current I exceeds the corresponding critical current I_c.

The conditions under which multiple resistive branches are observed in CVCs are related to both the independent dynamic behavior of each junction and the presence of hysteresis. The dynamic behavior of layered structures with Josephson coupling is thoroughly analyzed, e.g., in Refs [47] and [36] based on the model with a manifold of sequential Josephson junctions.

As in the common model of a Josephson junction at $I > I_c$, the authors of Ref. [47] and [36] determine the total current in the direction of the c-axis as a sum of Josephson, resistance, and capacitance currents between the layers of the structure. Indeed, in the general case, it is necessary to consider the resistive model of a Josephson junction considering the presence of capacitance effects in the system.

Resistive mode with capacitance. When constructing an equivalent circuit of a Josephson junction, presented in Fig. 6a, one more factor was not considered: the construction of the Josephson junction itself, in which two banks separated by an interlayer of dielectric resemble a capacitor and, therefore, the system must possess capacitance. Thus, the equivalent circuit in the framework of the resistive model is to be completed with a capacitor C connected in parallel. The generalized equivalent circuit of an individual Josephson junction for this case [44, 46] is shown in Fig. 7a.

Although no direct current through a capacitor is possible, an alternating displacement current $I_d = C\,dV/dt$ related to recharging the capacitor plates can flow through it. Analyses (see, e.g., [44, 46] for more details) show that the presence of capacitance in a Josephson junction leads to hysteresis in its current-voltage characteristic: the dependence $I(V)$ is different for the cases of increasing and decreasing I.

The hysteresis behavior of the current-voltage characteristic of a Josephson junction is shown in Fig. 7b. Quantitatively, the return current ('capture current' I_r) and the irreversibility of properties are determined by the magnitude of McCumber parameter [48]:

$$\beta = \left(\frac{2e}{\hbar}\right) I_c C R^2 . \tag{8}$$

When $\beta \ll 1$, the capacitance term can be ignored, while the current-voltage characteristic is reversible and has a form like the one in Fig. 6b. With growing β, the hysteresis arises with the return current I_r, which decreases with the growth of β; in the limit $\beta \to \infty$, we have $I_r \to 0$, meaning that in this limit the return part of the current-voltage characteristic becomes linear (see Appendix).

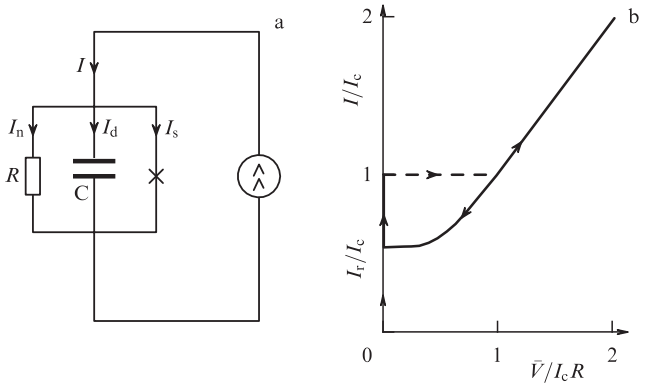

Figure 7. (a) Resistive model of a Josephson junction connected in a circuit to a current source, generalized to the case of capacitance. Total current I consists of superconducting current $I_s = I_c \sin\varphi$, normal dissipative current I_n, and displacement current through capacitor I_d. Josephson contact is indicated by an '×' [46]. (b) Current-voltage characteristic of a Josephson junction with capacitance $\beta = 5$. As current increases, voltage disappears at a capture current I_r that is less than I_c, i.e., hysteresis occurs [46].

3.2 Current-voltage characteristics of intrinsic Josephson junctions (experiment)

Multiple experiments on the intrinsic Josephson effect have been carried out to date. In this section, we will discuss some results obtained for stacks of intrinsic Josephson junctions in layered cuprate HTSCs. Attention will be focused on the processes of quasiparticle tunneling in both the superconducting and normal state.

The intrinsic Josephson effect caused by the tunneling of charge carriers in both superconducting and normal states of cuprate multilayer HTSCs has been intensely studied during recent decades. The distinctive feature of current-voltage characteristics for the current directed along the c-axis with a high (to a few hundred) number of hysteresis resistive branches most clearly manifests itself in the maximally anisotropic Bi and Tl systems [24, 35] (see also reviews [33, 34] and references therein).

Figure 8 presents the data from the paper by Heim et al. [34] on the intrinsic Josephson effect in the $Bi_2Sr_2CaCu_2O_8$ system. Properly prepared mesa structures on BSCCO single crystals act like stacks of intrinsic Josephson tunnel junctions.

The mesa structure presented in Fig. 8 contains $N = 5$ Josephson junctions; beyond the critical currents of these junctions, the CVC has 5 branches in the resistive state, differing by the resistive junction number (see the inset).

Yu et al. [37] developed a two-sided method of manufacturing a stack of intrinsic Josephson junctions, built in the volume of very thin ($d \leqslant 100$ nm) $Bi_2Sr_2CaCu_2O_{8+x}$ single crystals. The authors combine this method with high-accuracy control of etching to create structures with a not large ($N = 0 - 6$) number of intrinsic Josephson junctions, including the important case of a single junction. Figure 3 of Ref. [37] presents the CVCs of such structures with a sequentially increasing number of intrinsic Josephson junctions. In addition to the possibility of tunnel spectroscopy of the superconducting gap, this technique is also important for possible applications such as SQUID and high-frequency mixers.

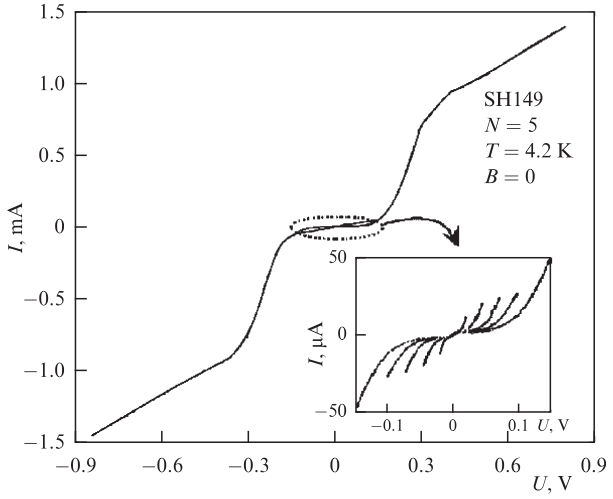

Figure 8. Current-voltage characteristic at 4.2 K of a 1×1-μm^2 BSCCO mesa structure containing 5 junctions. Inset shows same CVC on an enlarged scale [34].

As most experiments were devoted to the study of $Bi_2Sr_2CaCu_2O_8$ (BSCCO) systems, it was of particular importance to study a compound other than BSCCO to imagine the general picture.

The authors of Ref. [49] were the first to present intrinsic tunneling spectra of the $Bi_2Sr_{2-x}La_xCuO_{6+\delta}$ (BSLCO) system doped with La with a single CuO_2 layer. Despite a 3-fold difference between the optimal critical temperatures of superconductivity for BSLCO and BSCCO (32 K and 95 K, respectively) and, therefore, different spectral energy scales, the authors discovered a vividly expressed picture of tunnel spectra for a stack of intrinsic Josephson junctions.

Figure 9 shows current-voltage characteristics for an optimally doped BSLCO mesa structure with $T_c \approx 32$ K. At sufficiently small currents, there are $N = 18$ hysteresis branches, each of them corresponding to a sequential switching of more and more intrinsic tunnel junctions from the superconducting to the normal state.

When the bias current becomes greater than the superconductivity critical current $I_{c_{max}}$ of the last ('strongest') junction in the mesa structure, the CVC becomes single-valued. This single-valued curve corresponds to a sum of voltages at all N junctions.

In many papers, the importance of the McCumber parameter β [48] for the experimental manifestation of series of individual Josephson junctions in CVCs of multilayer superconductors is emphasized. Since the McCumber parameter reflects the capacitance of the Josephson junction, a large value of β is likely to promote individual switching of the Josephson junctions when, upon applying voltage, charge is dynamically induced in thin superconducting layers (see Appendix).

Estimates show that, for BSCCO, $\beta > 100$ and, therefore, multiple branches of intrinsic Josephson junctions as well as a large hysteresis effect can be observed even in mesa structures of BSCCO with sufficiently large dimensions [36].

Kleiner et al. [36] compared the form of CVCs in NTSC structures with substantially different values of β. Figure 10 shows an example of a current-voltage characteristic of a BSCCO single crystal with a critical current density of 140 A cm^{-2} at $T = 4.2$ K. The CVC demonstrates multiple branching, indicating that the coupling between different

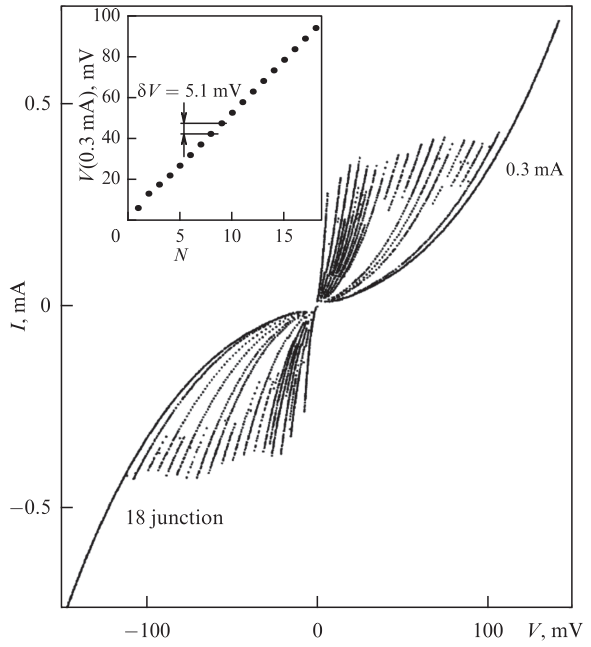

Figure 9. CVC for BSLCO mesa structure with intrinsic tunnel junctions ($N = 18$) at $T = 4.2$ K. Inset: voltage measured at 0.3 mA for each calculated branch ($N = 1 \ldots 18$). Linear dependence $V(N)$ with equidistant points testifies to homogeneity of Josephson junctions in mesa structure [49].

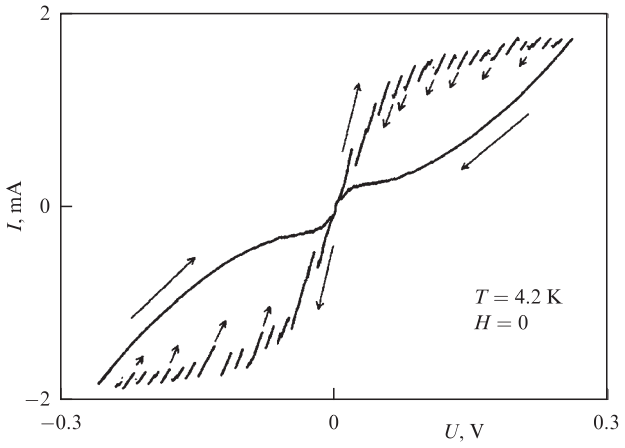

Figure 10. Current-voltage characteristic of BSCCO single crystal (annealed in Ar) having multiple quasiparticle branches [36].

Josephson junctions is small. The crystal thickness is 1.8 μm, and the sample consists of $N \approx 1200$ junctions.

In oxygen-annealed crystals having the composition $(Bi_{0.8}Pb_{0.2})_2Sr_2CaCu_2O_8$ (BSPCCO), a simultaneous switching of all junctions is actually observed (Fig. 11). For these crystals, the critical current density at $T = 4.2$ K amounts to 7 kA cm^{-2}, i.e., almost two orders of magnitude greater than for the BSCCO crystals annealed in Ar. The CVC in Fig. 11 can be described well using the value $\beta = 2.1$.

Thus, BSCCO single crystals annealed in Ar demonstrate multiply branched CVCs. On the contrary, the intrinsic Josephson junctions in PBSCCO single crystals annealed in oxygen switch to the resistive state simultaneously and are apparently strongly coupled. Such a behavior is largely determined by a sharp decrease in the McCumber parameter.

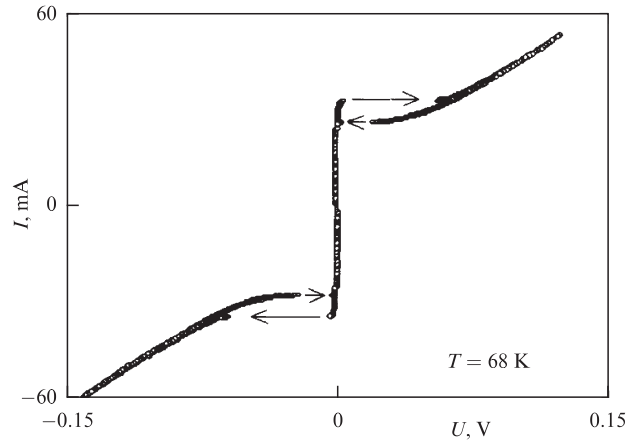

Figure 11. Current-voltage characteristic of BPSCCO single crystal (annealed in O_2) having only one resitive branch [36].

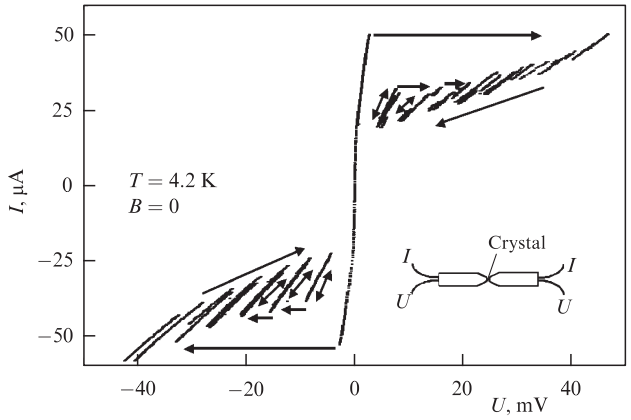

Figure 12. Current-voltage characteristics of single crystals of $RuSr_2GdCu_2O_8$ at currents applied in direction of c-axis. Schematic diagram of contacts to the sample is depicted in the inset [25].

Let us also consider examples of the manifestation of intrinsic Josephson effects in some 'exotic' layered HTSCs. Nachtrab et al. [25] explored the interlayer charge transport in low-sized (micrometer) single crystals of the magnetic superconductor $RuSr_2GdCu_2O_8$ (RSGCO). A clear intrinsic Josephson effect is found, showing that the material acts as a natural superconductor–insulator–ferromagnet–insulator–superconductor (SIFIS) superlattice.

The RuO_2 and CuO_2 layers are separated by layers of SrO, so that a natural multilayer SIFIS structure is formed, where I stands for SrO isolating layers, F corresponds to RuO_2 magnetic layers (with a weak ferromagnetic component), and S denotes the CuO_2 superconductor layers. In such a structure, the interlayer supercurrents between the neighboring layers of CuO_2 can be Josephson ones, like the interlayer supercurrents in BSCCO [35] or TBCCO [24] cuprates.

Figure 12 shows current-voltage characteristics at 4.2 K for one of the investigated RSGCO samples with $T_c = 51$ K in a zero magnetic field. A typical picture of multiple resistive branches with hysteresis properties is observed, known from observations of the intrinsic Josephson effect in cuprates. At a current of 50 A, the voltage jump δV is about 50 mV, which corresponds to the group of Josephson resistive junctions with $N = 2-3$.

Note that, when observing the intrinsic Josephson effect in a micron-sized single crystal of RSGCO in fields below 6 T, no nonstandard behavior due to the magnetism of RuO_2 layers is found.

Kawakami and Suzuki [50] studied the current-voltage characteristics of intrinsic Josephson junctions in electron-doped high-temperature superconductor $Sm_{2-x}Ce_xCuO_{4-\delta}$ (SCCO) using small-sized mesa structures (with cross-section area S) fabricated on the surface of a single crystal. It was found that the typical density of Josephson current I_c amounts to 7.5 kA cm^{-2} at 4.2 K for $T_c = 20.7$ K.

The CVC clearly shows resistive branching with $N \approx 60$, which correlates with the number of Josephson junctions in the mesa structure. This coincidence confirms that resistive branching originates from intrinsic Josephson junctions naturally embedded in the SCCO crystal structure, just as for p-type BSCCO.

From the S-dependence of CVCs of more than ten small mesa samples, it was concluded that the hysteresis and multiple resistive branching are observed only at S smaller than nearly 10 μm^2. This is a typical difference observed in CVCs when comparing mesa structures of different sizes.

For the McCumber parameter in SCCO with $S = 10$ μm^2, an estimate of $\beta = 2.86$ was obtained. Therefore, a small hysteresis of CVC can be expected in this structure. However, this value exceeds 1 by a small value only, so that it can change to a value smaller than 1 under a certain change of parameters. The closeness of β to 1 reflects the disappearance of hysteresis in current-voltage (I–V) characteristics of SCCO with an increase in the mesa structure size observed in this paper.

Figure 13 presents our data on CVCs for the electron-doped layered superconductor $Nd_{2-x}Ce_xCuO_4$ (NCCO) with $x = 0.15$. The measurements were carried out using optimally annealed epitaxial $Nd_{2-x}Ce_xCuO_4/SrTiO_3$ films 3500–4000 Å thick, obtained using the laser deposition method [51] with nonstandard orientation $(1\bar{1}0)$: the c-axis of the NCCO crystal lattice is directed along the long side of the $SrTiO_3$ substrate (Fig. 13a).

In the current-voltage characteristic [52] for a current along the c-axis in the region of weak currents (Fig. 13b), the signs of intrinsic Josephson junctions manifest themselves: $N = 3$ resistive branches are observed, separated by equal intervals $\delta U \approx 50$ mV at $I = 100$ A (see inset in Fig. 13b). According to preliminary estimates, this corresponds to a simultaneous transition of 4–5 Josephson junctions into the resistive state.

We presented a brief overview of basic physical concepts and considered examples of experimental manifestations of the intrinsic Josephson effect in strongly anisotropic layers of cuprate HTSCs. In this section, we restrict ourselves to considering the effects in a zero magnetic field. For a more complete picture of the phenomenon, see, e.g., the reviews by Yurgens [33] on the latest achievements in the study of intrinsic Josephson junctions and by Heim et al. [34] on the intrinsic tunnel effects in cuprates and manganites.

The intrinsic Josephson effect has been intensely studied during the last decade for the following reasons:

— the possibility of studying a number of fundamental phenomena;

— the use of intrinsic Josephson junctions for tunnel spectroscopy. Their advantage over external (artificial) tunnel junctions is that there is a possibility of 'probing' not only the surface layer but also all layers inside the structure;

— the voltage restricting high-frequency properties of intrinsic Josephson junctions is in the range of 30 mV, which

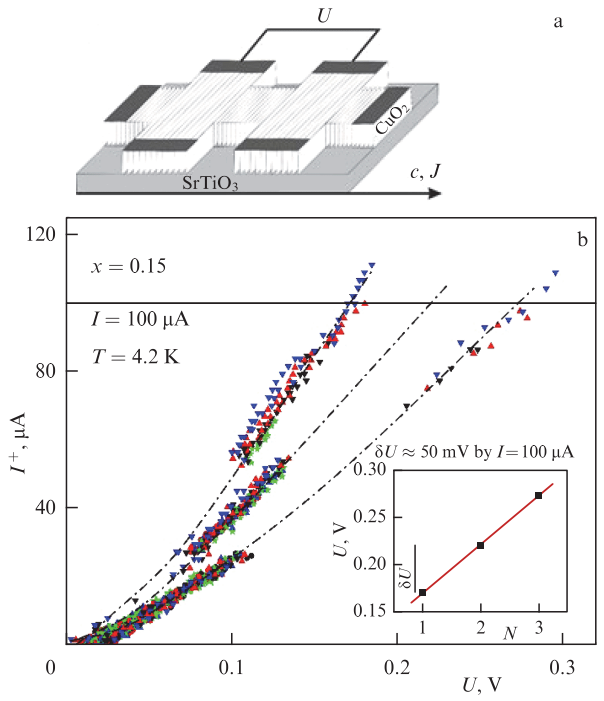

Figure 13. (a) Schematic of $Nd_{2-x}Ce_xCuO_4/SrTiO_3$ epitaxial film with orientation $(1\bar{1}0)$ [51]. (b) CVC for $Nd_{1.85}Ce_{0.15}CuO_4/SrTiO_3$ epitaxial film with intrinsic tunnel junctions ($N = 3$) at $T = 4.2$ K. Inset: voltage measured at 100 μA for each calculated branch ($N = 1, 2, 3$) [52].

allows alternating Josephson currents at frequencies of a few THz [53, 54]. Hence, such junctions are very promising for terahertz applications, such as generators or mixers.

The review by Kleiner and Wang [55] presents a thorough tutorial on terahertz radiation from many intrinsic Josephson junctions in layered $Bi_2Sr_2CaCu_2O_{8+x}$ crystals. The electromagnetic radiation in the terahertz (THz) range is of great interest for potential applications in biology or medical diagnostics, broadband communication, security and defense, nondestructive control, and other areas. However, in particular, the frequency range from 0.5 to 1.5 THz turns out to be difficult to fill with high-power coherent solid-state sources.

Structures appropriately made of the superconductor $Bi_2Sr_2CaCu_2O_{8+x}$ with a high critical temperature can operate at frequencies in the THz range, and the best devices at present reach an output power of about 100 μW.

In review [55], the reader can get acquainted with the basic physics of this type of oscillators, as well as with oscillator manufacturing, the measurement methods used for oscillator characterization, and models used to describe their dynamics, including a model based on the intrinsic Josephson effect. Examples are presented demonstrating the potential applications in terahertz imaging and terahertz spectroscopy.

4. Conclusions

It is currently assumed that the properties of layered cuprates with a high critical temperature in both the normal and superconducting states are determined by the properties of the CuO_2 layers, while other structural components in the unit cell act as charge reservoirs. In this model, the processes of charge carrier tunneling along the *c*-axis are relevant in both the superconducting (Cooper pair tunneling) and normal (single particle tunneling) states of the layered superconductor.

The combination of a nonmetallic type of temperature dependence of resistance along the *c*-axis with metallic conductivity in the *ab*-plane at a strong anisotropy of the conducting layers, $\rho_c/\rho_{ab} \gg 1$, is evidence of the quasi-two-dimensionality of oxide systems consisting of high mobility CuO_2 layers separated by buffer layers.

We presented experimental results on the nonmetallic temperature dependence of the resistance $\rho_c(T)$ for both hole-doped cuprates and the magnetic superconductor $RuSr_2GdCu_2O_8$ and pnictide $(V_2Sr_4O_6)Fe_2As_2$, as well as for the electron-doped cuprate $Nd_{2-x}Ce_xCuO_4$. The nonmetallic behavior of the $\rho_c(T)$ dependence and the large anisotropy of the resistance are determined by the incoherent tunneling of charge carriers in the direction of the *c*-axis in the natural superlattice model for the multilayer crystal structure of HTSC systems.

Due to the layered structure and strong anisotropy, a high temperature cuprate crystal in the superconducting state can be considered to be a set of successive tunneling Josephson junctions, called intrinsic Josephson junctions. The intrinsic Josephson effect as the tunneling of Cooper pairs between adjacent CuO_2 layers inside a highly anisotropic layered crystal is an integral part of modern concepts in the field of high-temperature superconductors.

We have considered examples of characteristic branched CVCs in the superconducting state as experimental manifestations of the intrinsic Josephson effect for mesa structures based on hole-doped $Bi_2Sr_2CaCu_2O_{8+x}$, $Bi_2Sr_{2-x}La_xCuO_{6+\delta}$, and $(Bi_{0.8}Pb_{0.2})_2Sr_2CaCu_2O_8$, electron-doped $Sm_{2-x}Ce_xCuO_{4-\delta}$ and $Nd_{2-x}Ce_xCuO_4$, as well as the magnetic superconductor $RuSr_2GdCu_2O_8$.

In this review, we restricted ourselves to considering effects in a zero magnetic field. Research in a magnetic field is an extensive and rapidly developing area of study of layered HTSCs, promising for practical applications. Here are some useful references on the study of the intrinsic Josephson effect in a magnetic field: Ooi-2002 [56], Machida-2003 [57], Kadowaki-2006 [58], Koshelev-2007 [59], Moll-2014 [23].

The key phenomenon associated with the Josephson effect is the oscillations of various properties of superconducting tunnel junctions with a magnetic field. To study the system of Josephson vortices in HTSC single crystals, resistance measurements are carried out in the vortex flow mode for a magnetic field parallel to the layers. New periodic oscillations of the flow resistance have been discovered in a wide range of temperatures and magnetic fields in $Bi_2Sr_2CaCu_2O_{8+y}$ single crystals [56, 58], as well as in the $(Sr_4V_2O_6)Fe_2As_2$ pnictide with the intrinsic Josephson effect [23].

In the framework of mesoscale modeling [57], as well as in the theoretical consideration of magnetic oscillations of the critical current in stacks of intrinsic Josephson junctions [59], it was shown that the observed periodic dependence is due to the dynamic matching of the Josephson vortex lattice with the edges of the sample (Josephson vortex commensurability oscillations).

Acknowledgments. The study was carried out with the financial support of the Ministry of Science and Higher Education (grant of 29.09.2020, no. 075-15-2020-797 (13.1902.21.0024)). The authors express their gratitude to A A Ivanov for manufacturing high-quality samples, as well as to A S Klepikova and E F Talantsev for their fruitful cooperation.

5. Appendix. McCumber parameter

An important parameter determining the type of current-voltage characteristic (CVC) of a Josephson junction with capacitance C is the McCumber (Stewart–McCumber) parameter, or hysteresis parameter, β, which is a measure of the current attenuation in the SIS junction [48, 60]. Generally, the value of β should be less than one to make the CVC not hysteretic.

Within the resistive model for the SIS junction, the total current I through the system is the sum of the superconducting current $I_s = I_c \sin\varphi$; the normal current $I_n = V/R$, where R is the junction resistance in the normal state, and the displacement current $I_d = C\,\mathrm{d}V/\mathrm{d}t$, associated with the recharging of the capacitor plates:

$$I = I_s + I_n + I_d\,. \tag{A.1}$$

Using the fundamental relationship of the Josephson effect theory [42] between the voltage across the junction and the rate of temporal change of the phase difference between the banks ($\varphi = \varphi_1 - \varphi_2$),

$$V(t) = \frac{\hbar}{2e}\,\frac{\partial\varphi}{\partial t}\,, \tag{A.2}$$

and multiplying both sides of (A.1) by $\hbar/2e$, we obtain the following equation:

$$\left(\frac{\hbar}{2e}\right)^2 C\ddot{\varphi} + \left(\frac{\hbar}{2e}\right)^2 \frac{1}{R}\,\dot{\varphi} + E_c \sin\varphi = E_c\,\frac{I}{I_c}\,, \tag{A.3}$$

determining the phase dynamics at a given current I through the junction. Here, $\ddot{\varphi}$ and $\dot{\varphi}$ denote the second-order and first-order time derivatives φ, $E_c = \hbar I_c/2e = \Phi_0 I_c/2\pi$, where $\Phi_0 = h/2e$ is the magnetic flux quantum.

All microscopic information about the junction is contained in the quantities I_c and R, while in the resistive model these quantities are considered given, and the behavior of the macroscopic characteristic of the junction is studied, namely, the phase difference φ, which characterizes the superconducting state of the junction in general.

Equation (A.3) is in fact the equation of motion of a pendulum under the action of a driving force and in the presence of friction [44, 46, 48, 60] (see, e.g., [61]): $\ddot{\varphi}$ and $\dot{\varphi}$ are the angular acceleration and angular velocity of the pendulum with the moment of inertia $J = (\hbar/2e)^2 C$, the coefficient of friction $\eta = (\hbar/2e)^2/R$, the gravitational moment $mgl = E_c$, and the applied torque $E_c\,(I/I_c)$.

Equation (A.3) can be written in a more compact form:

$$\beta\frac{\ddot{\varphi}}{\omega_c^2} + \frac{\dot{\varphi}}{\omega_c} + \sin\varphi = \frac{I}{I_c}\,, \tag{A.4}$$

where the notions of a characteristic Josephson frequency

$$\omega_c = \frac{2e}{\hbar}\,I_c R \tag{A.5}$$

and McCumber parameter [48]

$$\beta = \frac{2e}{\hbar}\,I_c C R^2 \tag{A.6}$$

are introduced.

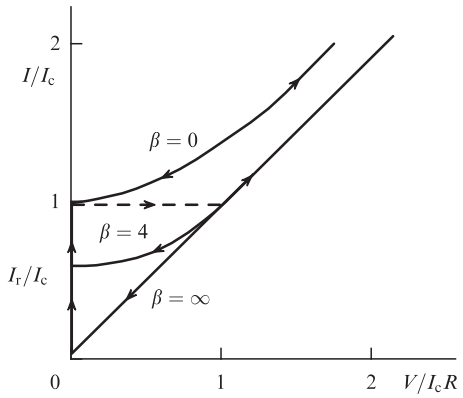

Figure 14. Current-voltage characteristics of a Josephson junction included in a circuit with a source of current I, calculated within the resistive model for cases of insignificant ($\beta = 0$), intermediate ($\beta = 4$), and dominant ($\beta = \infty$) capacitance [44, 46].

When $\beta \ll 1$, so that the capacitance term can be ignored, Eqn (A.4) for function $\varphi(t)$ is integrated in elementary functions, after which Eqn (A.2) yields

$$V(t) = R\frac{I^2 - I_c^2}{I + I_c\cos\omega t}\,, \qquad \omega = \frac{2e}{\hbar}\,R\sqrt{I^2 - I_c^2}\,. \tag{A.7}$$

The current-voltage characteristic of a Josephson junction mapped by DC instruments as an interrelation between I and the time-averaged voltage $\bar{V}$ in this case is reversible and has the form (7) $\bar{V} = R\sqrt{I^2 - I_c^2}$ (see Fig. 6b and the upper curve in Fig. 14).

The numerical solution of Eqn (A.4) using (A.2) shows that, with an increase in β, the presence of capacitance in the Josephson junction leads to an ambiguous form of its current-voltage characteristic: the dependence $V(I)$ becomes different for the cases of increasing and decreasing I (Fig. 7b). With an increase in the current, the voltage appears through a jump at $I \geqslant I_c$, whereas, on decreasing the current, the voltage disappears at the capture current I_r, which is less than I_c, i.e., hysteresis takes place.

Quantitatively, the capture (return) current and the hysteresis properties are determined by the value of the McCumber parameter (see Figs 14 and 15). The value of I_r decreases with an increase in β, and in the limit $\beta \to \infty$ tends to zero. In this limit, the return part of current-voltage characteristic becomes linear, which means effective suppression of the superconducting component of the current through the junction.

Stewart [60] thoroughly considered the model of superconducting Josephson junctions with capacitance, similar to the model of simple driven pendulum with damping. Careful analysis has shown that this model yields CVC curves demonstrating hysteresis properties.

Dissipation processes (normal resistance) in the junction and the capacitance value determine the reversibility (or irreversibility) of the $I-V$ curve.

The equation for the total current through a Josephson contact, in addition to the superconducting component of the current through the junction, considers the displacement current through the shunting capacitance C of the junction, as well as 'normal' losses represented by the shunting resistor R:

$$\ddot{\varphi} + \frac{\dot{\varphi}}{\tau} + \varphi_0^2 \sin\varphi = \omega_0^2\,\frac{I}{I_c}\,. \tag{A.8}$$

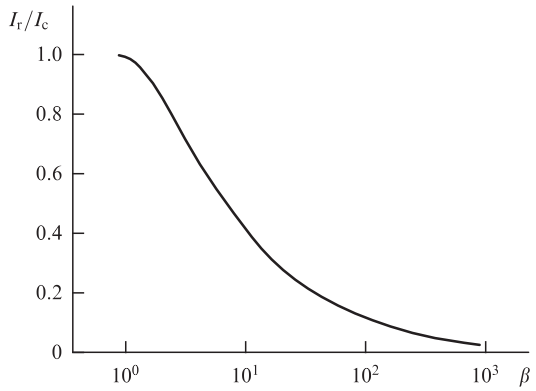

Figure 15. Dependence of return current on value of parameter β [44].

Here, $\tau = RC$ is the damping time, and the frequency $\omega_0 = \sqrt{2eI_c/\hbar C} = \sqrt{2\pi I_c/C\Phi_0}$ in the Josephson case is called the plasma frequency of the junction. The plasma frequency can also be considered the resonance frequency of the corresponding pendulum. The relation between the notations in Eqns (A.8) and (A.4) is as follows:

$$\omega_0^2 = \frac{\omega_c^2}{\beta}, \quad \omega_c\tau = \beta, \quad \text{and} \quad \omega_0\tau = \sqrt{\beta}.$$

The DC current-voltage $(I-\bar{V})$ characteristics, calculated in Ref. [60] by means of Eqn (A.8) for the set of $\omega_0\tau$ parameter values, are presented in Fig. 16.

The CVC curves corresponding to the direct Josephson current at $I/I_c \leqslant 1$ ($\ddot{\varphi} = \dot{\varphi} = 0$ and $\varphi = \arcsin(I/I_c)$ in (A.8)) are reversible and have the form (7) $\bar{V} = R\sqrt{I^2 - I_c^2}$. However, the curve $(I-\bar{V})$ has a reversible form only at $\omega_0\tau \leqslant 0.5$.

For intermediate values of $\omega_0\tau$, the solutions obtained by numerical integration of Eqn (A.8) lead to the CVCs presented in Fig. 16: at $\omega_0\tau > 1$, dependences become irreversible with abrupt horizontal jumps of the voltage to zero under the current decrease, i.e., hysteresis effects take place. For $\omega_0\tau \gg 1$, the $(I-\bar{V})$ dependence tends to the origin of coordinates following a linear law, which indicates suppression of Josephson supercurrent in this situation.

All the above concerns a single Josephson junction. At the same time, as is shown by the data set on the Intrinsic Josephson effect in multilayered HTSCs, the value of the McCumber parameter plays an essential role in experimental manifestations of CVC branches for the junctions of individual layers in these systems (see Section 3.2).

Indeed, the structure of current-voltage characteristics for the current along the *c*-axis with a large (up to a few hundred) number of hysteresis resistive branches most clearly manifests itself in strongly anisotropic layered Bi and Tl systems [24, 35] (see also reviews [33, 34] and references therein). Estimates show that for BSCCO $\beta > 100$ and, consequently, there are multiple branches of intrinsic Josephson junctions, and that a large hysteresis effect in current-voltage characteristics can be observed even in BSCCO mesa structures of substantially large sizes [36].

The dynamic behavior of layered structures with Josephson coupling is thoroughly analyzed, e.g., in Refs [36] and [47] based on the model with multiple sequential Josephson junctions. It was shown that the conditions under which multiple resistive branches are observed on CVCs are due to both the independent dynamic behavior of each junction and the presence of hysteresis. Since the McCumber parameter reflects the capacitance of a Josephson junction, in the presence of voltage, a large value of β promotes dynamic charge induction in thin superconducting layers and, consequently, individual switching of Josephson junctions.

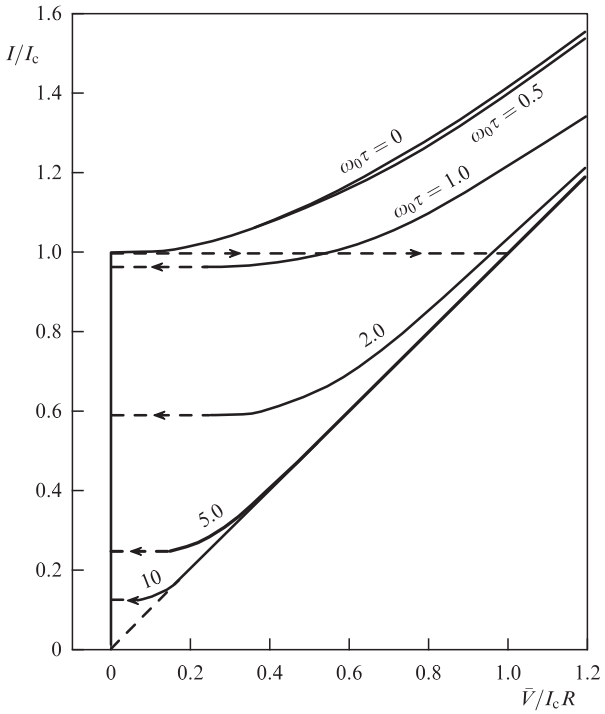

Figure 16. Curves of dependence of normalized direct current through a junction on the voltage, calculated according to (A.8) for different values of parameter $\omega_0\tau(=\sqrt{\beta})$. Solid sections of curves are reversible; intermittent jumps are shown by dashed lines with arrows [60].

References

1. Plakida N M *High-Temperature Superconductivity: Experiment and Theory* (Berlin: Springer, 2012) eBook, https://doi.org/10.1007/978-3-642-78406-4
2. Kopnin N B *Theory of Nonequilibrium Superconductivity* (New York: Oxford Univ. Press, 2009)
3. Tinkham M *Introduction to Superconductivity* (New York: Dover Publ., 2004)
4. Poole C P et al. *Superconductivity* (Waltham, MA: Elsevier, 2014)
5. Lawrence W E, Doniach S, in *Proc. of the 12th Intern. Conf. on Low Temperature Physics, Kyoto, 1970* (Ed. E Kanda) (Tokyo: Keigaku, 1971) p. 361
6. Bulaevskii L N *Sov. Phys. JETP* **37** 1133 (1973); *Zh. Eksp. Teor. Fiz.* **64** 2241 (1973)
7. Bulaevskii L N et al. *Phys. Rev. B* **53** 14601 (1996)
8. Blatter G et al. *Rev. Mod. Phys.* **66** 1125 (1994)
9. Tozer S W et al. *Phys. Rev. Lett.* **59** 1768 (1987)
10. Hagen S J et al. *Phys. Rev. B* **37** 7928 (1988)
11. Penney T et al. *Phys. Rev. B* **38** 2918 (1988)
12. Friedmann T A et al. *Phys. Rev. B* **42** 6217 (1990)
13. Nakamura Y, Uchida S *Phys. Rev. B* **47** 8369 (1993)
14. Kao H L et al. *Phys. Rev. B* **48** 9925 (1993)
15. Takagi H et al. *Phys. Rev. B* **40** 2254 (1989)
16. Martin S et al. *Phys. Rev. B* **41** 846 (1990)
17. Anderson P W, Zou Z *Phys. Rev. Lett.* **60** 132 (1988)
18. Kotliar G et al. *Europhys. Lett.* **15** 655 (1991)
19. Sadovskii M V *Superconductivity and Localization* (Singapore: World Scientific, 2000) https://doi.org/10.1142/4321
20. Ito T et al. *Nature* **350** 596 (1991)
21. Rapp M et al. *Phys. Rev. Lett.* **77** 928 (1996)

22. Popov M R et al. *Mater. Res. Express* **6** 096005 (2019)
23. Moll P J W et al. *Nature Phys.* **10** 644 (2014)
24. Kleiner R, Müller P *Phys. Rev. B* **49** 1327 (1994)
25. Nachtrab T et al. *Phys. Rev. Lett.* **92** 117001 (2004)
26. Cassam-Chenai A, Mailly D *Phys. Rev. B* **52** 1984 (1995)
27. McKenzie R H, Moses P *Phys. Rev. Lett.* **81** 4492 (1998)
28. Kapaev V V, Kopaev Yu V *JETP Lett.* **68** 223 (1998); *Pis'ma Zh. Eksp. Teor. Fiz.* **68** 211 (1998)
29. Giura M et al. *Phys. Rev. B* **68** 134505 (2003)
30. Giura M et al. *Physica C* **460 – 462** 831 (2007)
31. Charikova T B et al. *J. Theor. Exp. Phys.* **105** 626 (2007); *Zh. Eksp. Teor. Fiz.* **132** 712 (2007)
32. Anderson P W *The Theory of Superconductivity in the High-T_c Cuprates* (Princeton, NJ: Princeton Univ. Press, 1997)
33. Yurgens A A *Supercond. Sci. Technol.* **13** R85 (2000)
34. Heim S et al. *Physica C* **367** 348 (2002)
35. Kleiner R et al. *Phys. Rev. Lett.* **68** 2394 (1992)
36. Kleiner R et al. *Phys. Rev. B* **50** 3942 (1994)
37. You L X et al. *Appl. Phys. Lett.* **88** 222501 (2006)
38. Ding J F et al. *J. Appl. Phys.* **108** 123903 (2010)
39. Schlenga K et al. *Physica C* **235 – 240** 3273 (1994)
40. Kawakami T, Suzuki M *Phys. Rev. B* **76** 134503 (2007)
41. Schlenga K et al. *Phys. Rev. B* **57** 14518 (1998)
42. Josephson B D *Phys. Lett.* **1** 251 (1962)
43. Likharev K K *Rev. Mod. Phys.* **51** 101 (1979)
44. Schmidt V V *The Physics of Superconductors*: *Introduction to Fundamentals and Applications* (Eds V V Schmidt, P Müller, A V Ustinov) (Berlin: Springer, 1997) translated from 1st Russian ed.; Shmidt V V *Vvedenie v Fiziku Sverkhprovodnikov* 2nd ed., rev. and enlarg. (Introduction to the Physics of Superconductors) (Moscow: MTsNMO, 2000)
45. Tafuri F (Ed.) *Fundamentals and Frontiers of the Josephson Effect* (Springer Series in Materials Science, Vol. 286) (Cham: Springer, 2019) https://doi.org/10.1007/978-3-030-20726-7
46. Fominov Ya V, Shchelkachev N M (Compil.) *Effekt Dzhozefsona*: *Uchebno-metodicheskoe Posobie* (Josephson Effect: A Tutorial) (Moscow: MFTI, 2010)
47. Sakai S, Bodin P, Pedersen N F *J. Appl. Phys.* **73** 2411 (1993)
48. McCumber D E *J. Appl. Phys.* **39** 3113 (1968)
49. Yurgens A et al. *Phys. Rev. Lett.* **90** 147005 (2003); cond-mat/0212562
50. Kawakami T, Suzuki M *Phys. Rev. B* **76** 134503 (2007)
51. Ivanov A A et al. *Physica C* **180** 69 (1991)
52. Charikova T B et al. *Nanofizika i Nanoelektronika. Trudy XXVII Mezhdunarodnogo Simpoziuma* (Nanophysics and Nanoelectronics Proc. of the XXVII Intern. Symp.) Vol. 1 (Nizhny Novgorod: IPF RAN, 2023) pp. 123–124
53. Rother S et al. *Physica C* **341 – 348** 1565 (2000)
54. Rother S et al. *IEEE Trans. Appl. Supercond.* **11** 1191 (2001)
55. Kleiner R, Wang H *J. Appl. Phys.* **126** 171101 (2019)
56. Ooi S, Mochiku T, Hirata K *Phys. Rev. Lett.* **89** 247002 (2002)
57. Machida M *Phys. Rev. Lett.* **90** 037001 (2003)
58. Kadowaki K et al. *Physica C* **437 – 438** 111 (2006)
59. Koshelev A E *Phys. Rev. B* **75** 214513 (2007)
60. Stewart W C *Appl. Phys. Lett.* **12** 277 (1968)
61. Landau L D, Lifshitz E M *Mechanics* (Oxford: Pergamon Press, 1976); Translated from Russian: *Mekhanika* (Moscow: Fizmatlit, 2004)